Infection dynamics and virulence potential of clinical *Pseudomonas aeruginosa* isolates in a human airway epithelium model system

Claudia Antonella Colque[1,#,*], Signe Lolle[1,#], Ruggero La Rosa[1,*], Maria Pals Bendixen[1], Filipa Bica Simões[1], Kasper Aanæs[2,3], Søren Molin[4], Helle Krogh Johansen[1,2*].

[1] Department of Clinical Microbiology 9301, Rigshospitalet, 2100 Copenhagen Ø, Denmark

[2] Department of Clinical Medicine, Faculty of Health and Medical Sciences, University of Copenhagen, 2200 Copenhagen, Denmark.

[3] Department of Otorhinolaryngology, Head and Neck Surgery & Audiology, Rigshospitalet, 2100 Copenhagen Ø, Denmark.

[4] The Novo Nordisk Foundation Center for Biosustainability, Technical University of Denmark, 2800 Kgs. Lyngby, Denmark.

# These authors contributed equally.

* Corresponding authors: Claudia Antonella Colque (antcol@biosustain.dtu.dk), Ruggero La Rosa (rugros@dtu.dk), Helle Krogh Johansen (hkj@biosustain.dtu.dk).

Abstract

Persistent bacterial infections constitute an increasing health problem, which is often associated with antibiotic resistance. However, investigations of chronic lung inflammation and persistent infections with *Pseudomonas aeruginosa* in people with cystic fibrosis (pwCF) show that treatment failures may instead be rooted in host-microbe interactions developing after bacterial colonization of the CF airways. Using a laboratory infection model based on human airway epithelial tissues, cultured in an Air-Liquid Interface (ALI) system, we simulated the infection process of various *P. aeruginosa* strains to investigate the colonisation dynamics and the virulence potential during infection of nasal epithelial cultures from both non-CF and CF donors in addition to an immortalized bronchial cell line, BCi-NS1.1. Infections by *P. aeruginosa* reference strains and clinical isolates from pwCF were employed. While reference and patients' early strains exhibited high virulence and increased epithelial disruption, clinically adapted strains showed reduced virulence potential and limited epithelial damage regardless of the host cell type or clonal lineage. Dual RNA-seq analysis revealed that colonization of ALI cultures with virulent PAO1 significantly upregulated inflammatory pathways in host cells, an effect that was dampened in the less virulent *pscC* mutant strain lacking the type III secretion system. Simultaneously, while bacterial gene expression was similar in wild-type and BCi-NS1.1 cultures, in CF cells, the *pscC* strain showed dysregulation of genes involved in iron starvation, respiration, and quorum sensing pathways. Altogether, our results summarize the infection dynamics in the ALI model system and in pwCF, and provide a snapshot of the interplay between the airway epithelium and *P. aeruginosa*.

Introduction

With increasing lifespans and changes in lifestyle, persistent bacterial infections are on the rise [1]. Although antibiotics are generally effective, diagnosing and treating these infections is often challenging because of their complexity and the continuous changes in both the host and pathogen [2]. This is worsened by the lack of robust and reliable model systems to predict infection outcomes and treatment efficacy. However, by understanding treatment failures in relevant model systems, better diagnostics and therapies can be developed.

People with cystic fibrosis (pwCF) often suffer from persistent bacterial infections caused by a plethora of bacterial pathogens that colonize the airways and persist for decades. CF is caused by mutations in the cystic fibrosis transmembrane conductance regulator protein (CFTR), which is crucial for fluid homeostasis [3]. CFTR mutations result in impaired chloride secretion, increased mucus viscosity and reduced cilia beating, ultimately leading to mucociliary clearance [4]. This creates the perfect environment for pathogenic bacteria, such as *Pseudomonas aeruginosa*, which is the leading cause of respiratory morbidity and mortality in pwCF [5,6]. Recent advances in CFTR modulator therapies, particularly elexacaftor/tezacaftor/ivacaftor (ETI), significantly improve clinical well-being in pwCF by correcting and potentiating the function of the CFTR channels [7]. In addition, decreases in bacterial pathogen counts during ETI treatment have been shown [8]. However, *P. aeruginosa* persists in most patients, indicating the need for a deeper understanding of the relationship between ETI treatment and *P. aeruginosa* infections in pwCF [9–11].

Early infections are caused by environmental *P. aeruginosa* strains which adapt, over the years, to the CF environment through genetic, metabolic, and phenotypic changes [12,13]. This enhances antibiotic resistance, immune system evasion and a biofilm lifestyle and reduces virulence factor production [14–17]. In most patients, the initial clone drives within-host adaptation. Person-to-person transmission has also been documented in pwCF, and especially *P. aeruginosa* clones such as the DK01 and DK02 (Denmark), and high-frequent clones such as the C clone (ST17 clone, present in Europe and North America and persistent in pwCF) and PA14 (ST253 clone, found worldwide with affinity to CF and non-CF infections) have this capability [18–24]. However, how colonization and infection dynamics evolve during infection from a *P. aeruginosa*-human airway point of view remains largely unclear. This includes 1) the role of virulence factors, toxins, and specific dominant strains in tissue invasion and immune escape, 2) the epithelial responses and long-term effects on epithelial integrity and function,

87 and 3) how modulator treatment changes the infection pattern and the interaction between
88 the airway epithelium and the pathogen. Understanding the early stages of colonization,
89 therefore, may shed light on the bacterial pathogenic potential, antibiotic treatment failure,
90 and allow exploration of new treatment options. In addition, the lack of reliable *in vitro* model
91 systems which recreate the infectious microenvironment for studying infection processes in
92 the airway limits our understanding of colonization dynamics and bacterial virulence potential
93 within human tissue [25].

94 Various model systems including immortalized cell lines, primary cells, tissue explants,
95 and animal models have been created to study *P. aeruginosa*-human airway interactions [26].
96 3D air-liquid interface (ALI) airway tissue cultures closely mimic the human airway epithelium,
97 exhibiting differentiation, cell polarity, mucus production, and ciliary beating, which are
98 fundamental for understanding infection dynamics and colonization processes [27,28].
99 Nevertheless, only few studies have used ALI systems to shed light on bacterial infection
100 processes, resistance mechanisms and metabolic adaptation [16,29–34]. However, these studies
101 have used laboratory strains which do not reflect the complexity of clinical CF isolates and
102 their infection dynamics.

103 In this study, we used ALI cultures to profile *P. aeruginosa* infection using 12 clinical
104 strains from frequent and distinct lineages and compared them with standard reference
105 strains. We determined the overall physiological tissue response to the bacterial infections,
106 such as epithelial integrity, cytotoxicity, cytokine secretion, and bacterial colonization patterns
107 in infections of primary non-CF and CF nasal epithelial cells, and the bronchial cell line BCi-
108 NS1.1, as well as the impacts of the CFTR modulator, ETI. Dual RNA-seq revealed host and
109 bacterial response at the molecular level, unfolding their interactions. Our results investigate
110 early infection stages of airway epithelium and highlight the importance of host-pathogen
111 model systems to understand infection dynamics and develop new advanced therapies.

112

113 **Results**

114 *Host responses upon bacterial infections in ALI airway culture models*

115 To study the early dynamics of epithelial colonization, and to determine whether epithelial
116 tissues from different hosts exhibit individual responses upon *P. aeruginosa* infections, we
117 performed bacterial infection assays using a model system of airway epithelial cells grown
118 under ALI conditions (Fig S1). Specifically, we evaluated infection capabilities and epithelial

119 responses, using differentiated primary nasal cells from pwCF (n = 7) and non-CF (n = 3) donors
120 along with the human non-smoker immortalized bronchial BCi-NS1.1 cell line [35] infected with
121 a panel of *P. aeruginosa* strains (Fig S1, Table S1). Specifically for each infection, we quantified
122 bacterial proliferation and epithelium responses by measuring: 1) the transepithelial electrical
123 resistance (TEER) to quantify the integrity and permeability of the epithelium, 2) the release
124 of lactate dehydrogenase (LDH) in the basolateral media to quantify the induced epithelial cell
125 lysis, 3) the secretion of the chemokine Interleukin-8 (IL-8) to quantify the onset of
126 inflammation, and 4) the bacterial colony-forming units (CFU) (Table S2: Infection dynamics).
127 Infections were carried out using a collection of early (*_E), intermediate (*_I) and late (*_L)
128 clinical isolates from pwCF belonging to distinct clone types (lineages which differ by >10,000
129 SNPs), which comprise different stages of CF adaptation, evolutionary histories and infection
130 scenarios [36,37]. These clone types were chosen based on their frequency in the Copenhagen
131 CF Clinic (DK01 and DK02) and worldwide (C and PA14 clone, DK06 and DK19 clones in
132 Denmark, respectively). In addition, we included standard *P. aeruginosa* reference strains
133 (PAO1 and PA14), including a PAO1 derivative lacking the virulence determinant T3SS (*pscC*),
134 which is involved in host colonization, invasion and cell damage [32] (Table S1). It has been
135 shown that the Type III secretion plays an important role in the transition from acute to
136 chronic/persistent infection occurring during host adaptive evolution [38,39]. The chosen
137 bacteria exhibit distinct phenotypes, with laboratory and early strains characterized by high
138 growth rates and motility, whereas intermediate and late strains were characterized by slower
139 growth, reduced motility and mild-to-high increased minimum inhibitory concentration (MIC)
140 to tobramycin, ciprofloxacin and ceftazidime (Fig S2). To account for the varying growth rates
141 among strains (Fig S2C) and to ensure a comparable bacterial count at the end of the infections
142 regardless of strain or cell type, infections were conducted for 14 h for laboratory, early, and
143 intermediate strains, and for 38 h for late strains (DK01_L, DK02_L, DK06_L, and DK19_L). All
144 infection data are detailed in Table S2.

145 Consistent with the experimental set-up, no significant differences in CFUs were
146 observed across bacterial strains and ALI models on the apical (non-attached) side, as well as
147 the combined CFUs (total CFU) from all ALI compartments (Kruskal-Wallis followed by Dunn's
148 post-hoc test, $p>0.05$) (Fig S3). Additionally, Pearson's correlation analysis showed no
149 significant correlation between the total CFU relative to TEER drop (r=-0.27, p=0.0010), LDH
150 release (r=-0.004, p=0.9601), and IL-8 secretion (r=0.12, p=0.1441), indicating independence

151 of the variables. In addition, strain-specific bacterial infection outcomes (TEER drop,
152 compartment distribution, LDH release and IL-8 secretion) were generally comparable across
153 BCi-NS1.1, non-CF and CF models (Kruskal-Wallis followed by Dunn's post-hoc test, $p>0.05$),
154 except for DK01_L, DK06_L and DK19_L infections, where LDH released in CF was significantly
155 higher compared to non-CF models (Kruskal-Wallis followed by Dunn's post-hoc test, $p<0.01$,
156 Table S2: Infection Dynamics). In all cases, Pearson correlation analysis of infection data across
157 the different ALI models showed values > 0.9 ($p<0.001$) (Fig 1A). This suggests that in our
158 model system, the infection outcomes are mostly dependent on the specific virulence
159 potential of the infecting bacteria rather than conditional to the origin of the host sample.

160 When comparing across all infections (ALI, n = 194) to increase statistical power, the
161 TEER measurements at time 0 prior to each infection revealed tissue dependent values, with
162 BCi-NS1.1 cultures exhibiting the highest TEER followed by CF and non-CF primary cultures
163 (Kruskal-Wallis followed by Dunn's post-hoc test, $p<0.0001$) (Fig 1B). Similarly, CF cultures
164 exhibited the highest level of cellular damage (LDH release) and highest inflammatory
165 response (IL-8 secretion) (Kruskal-Wallis followed by Dunn's post-hoc test, $p<0.01$) (Fig 1C, D).
166 Comparable results were obtained when discriminating by the duration of infection (14 h vs
167 38 h) and control treatment (mock) (Fig S4). Moreover, CF cultures exhibited a time-
168 dependent increase of LDH release, underlining the intrinsic fragility of this tissue culture
169 (Kruskal-Wallis followed by Dunn's post-hoc test, $p<0.01$) (Fig S4D).

170 Next, we evaluated whether ETI treatment altered *P. aeruginosa* infection patterns in
171 the ALI system using primary cells from pwCF and non-CF controls (Table S2: ETI treatment).
172 As expected, 24 hours of ETI treatment resulted in a significant decrease in TEER (paired two-
173 sided t-test, $p<0.0001$) and an increase in transepithelial electrical conductance (TEEC) in CF
174 cells (paired two-sided t-test, $p<0.01$), indicating a treatment response (Fig 2A, B). No effect
175 was observed in non-CF cells (Fig S5C, D). This was confirmed by immunofluorescence staining
176 of the CFTR protein, allowing for a comparison between the ETI-treated and untreated ALI
177 cultures (Fig 2E). Infection outcomes in ETI-treated and untreated ALI cultures after 14h or
178 38h of infection using the PAO1 laboratory strain and the DK01_I and DK02_L clinical strains
179 showed no differences in TEER, bacterial growth or compartmental distribution of bacteria
180 when comparing different strains, ALI models, or ETI-treatment (Fig 2C, D and Fig S5).

181 These results suggest that in our ALI system, early infection dynamics are independent
182 of the cell type or treatment and may depend on other factors such as the specific bacterial

183 lineage, activation of the immune system, antibiotic treatments or change in mucus
184 composition, viscosity, and/or clearance which are currently not possible to recreate in the
185 ALI infection model system used. However, intrinsic differences between host cells such as
186 LDH release and IL-8 secretion, should be considered based on the specific requirements.
187

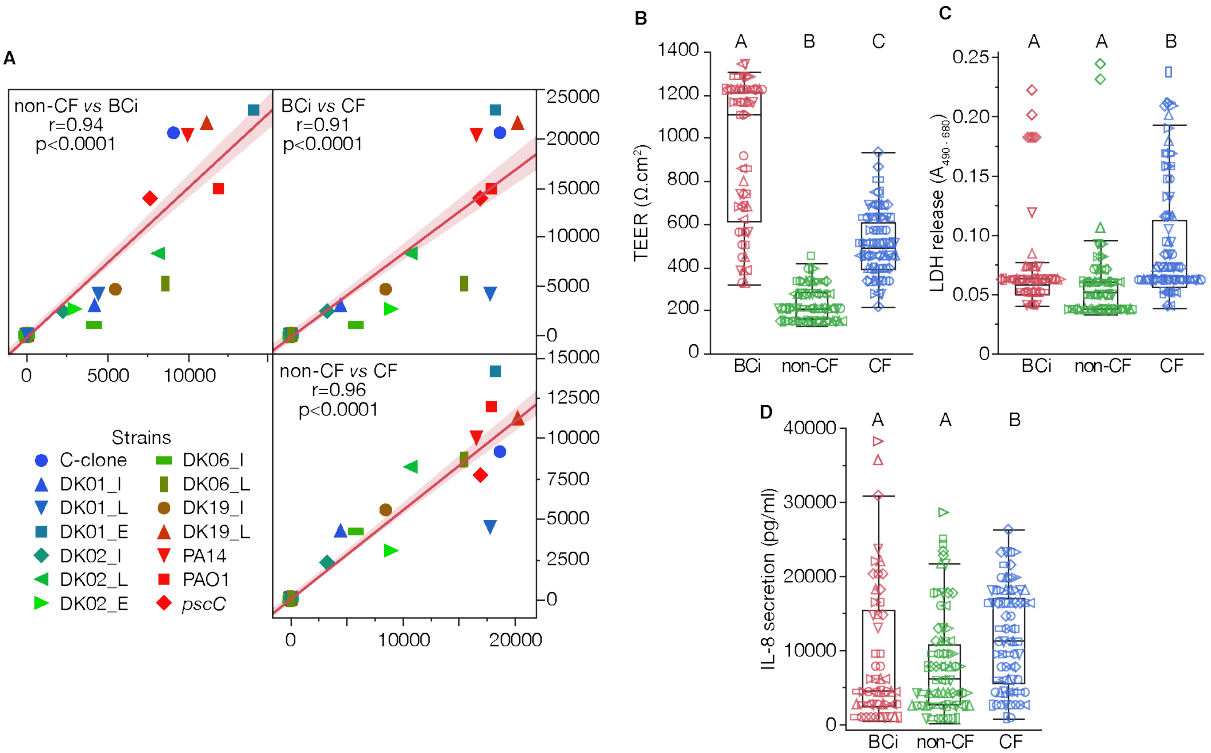

188

189 **Fig 1. Infection outcomes across ALI tissue types and bacterial strains.** A) Pearson correlation
190 analysis of the infection data across cultures and bacterial strains. Pearson's correlation
191 coefficient r, statistical significance (p value), linear fitting between the variables and 95%
192 confidence interval are indicated in the graph. B) TEER measurements of BCi-NS1.1, non-CF
193 and CF cultures after 28 days of differentiation in absence of bacterial infections. C) LDH
194 release by BCi-NS1.1, non-CF and CF airway cultures after 14 or 38 h of infections indicating
195 cytotoxicity post infection. D) IL-8 secretion in the basolateral media by BCi-NS1.1, non-CF and
196 CF cultures 14 or 38 hours post infection indicating a state of inflammation. Infections were
197 carried out at 14 h for early and intermediate strains of DK01, DK02, DK06 and DK19 and
198 laboratory strains PAO1 and PA14 and 38 h for late strains of DK01, DK02, DK06 and DK19. In
199 B, C and D, statistical significance was computed by Kruskal-Wallis followed by Dunn's post-
200 hoc test, where connecting letters report significance between groups ($p<0.05$). CF: cystic

201 fibrosis; BCi: BCi-NS1.1; TEER: transepithelial electrical resistance; LDH: lactate
202 dehydrogenase; IL-8: interleukin 8.
203

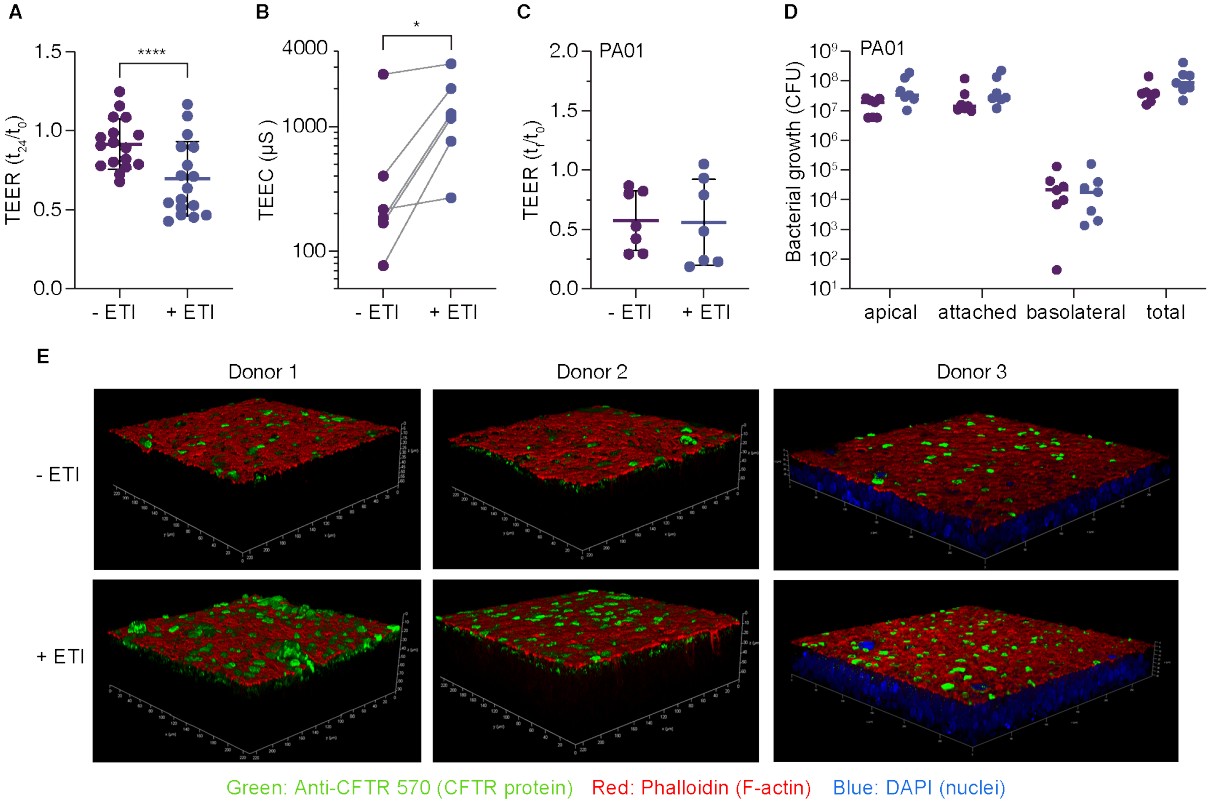

204

205 **Fig 2. Effect of elexacaftor/tezacaftor/ivacaftor (ETI) treatment on cystic fibrosis**
206 **transmembrane conductance protein (CFTR) function and infection pattern in** cystic fibrosis
207 (CF) cultures**.** A) Fold change in TEER measurements after 24 hours of ETI treatement (+ ETI)
208 or no treatement (- ETI) in ALI cultures from three CF donors homozygous for ΔF508 mutation.
209 B) TEEC after CFTR stimulation in treated (+ ETI) and untreated (- ETI) cells. Each dot represents
210 one independent donor. C) TEER change after 14 h of infection with PAO1 laboratory strain in
211 treated (+ ETI) and untreated (- ETI). D) Bacterial growth (CFU) after 14 h of infection in the
212 apical (non attached / free bacteria), attached to the epithelium, and basolateral
213 compartment, along with the total number of bacteria. In A,C-D, each dot represents one
214 independent experiment and the mean ± SD is included. Statistical significance was calculated
215 by paired two-sided t-test where **p<0.01 and ****p<0.0001. E) Three-dimensional
216 reconstruction of confocal microscopy images of immunofluorescent staining of CFTR protein
217 in ALI cultures from the CF donors treated (+ ETI) and untreated (- ETI). Green: Anti-CFTR 570
218 (CFTR protein), Red: Phalloidin (F-actin), Blue: DAPI (nuclei). ALI: air-liquid interface; TEER:

219 transepithelial electrical resistance; TEEC: transepithelial electrical conductance; CFU: colony-
220 forming units.
221
222 *Strain-specific infection phenotypes of* P. aeruginosa
223 After years of adaptive evolution in pwCF, *P. aeruginosa* changes its phenotype in response to
224 the host environment, including its stresses (e.g. antibiotics, ROS) and host components (e.g.
225 immune cells) [23,40]. Therefore, we aimed to evaluate if differences in strain adaptive evolution
226 and historical contingency restricted the infection capabilities in a convergent manner. Given
227 that bacterial infections progressed similarly across the different cell lines or ETI treatment,
228 for each strain, we averaged by their median the infection data in BCi-NS1.1, non-CF and CF
229 cultures (Table S2: Infection dynamics Avg.).
230 PCA and K-Means clustering identified four clusters of strains with similar infection
231 properties which can be associated with their virulence and evolutionary stage (Fig 3A).
232 Clusters 1 and 2 correspond to mostly virulent strains characterized by a substantial drop in
233 TEER, increased cytotoxicity (LDH release) and inflammation (IL-8). Contrarily, strains in
234 clusters 3 and 4 show a TEER close to the mock samples, which suggests reduced virulence
235 (Fig 3A, B). Therefore, PC 1 (50% of the variance), clusters strains based on their virulence
236 potential (defined as changes in TEER, LDH and IL-8 variables), while PC 2 (36.2% of the
237 variance) separates strains based on their ability to penetrate the epithelium. Strains from
238 cluster 1, indeed, even at a very low percentage, are found in the basolateral compartment of
239 the ALI cultures, indicating increased penetration through the epithelial layer. Strains from
240 cluster 3 are, instead, found at a lower percentage non-attached/free on the apical side and
241 preferentially attached to the cells either apically or internally (Fig 3). It is worth noting that
242 while the recombinant strain *pscC* and the DK02_L isolate were grouped in cluster 1 and
243 cluster 2, respectively, they show intermediate infection capabilities such as intermediate
244 TEER drop and relatively low LDH and IL-8 release as in clusters 3 and 4 (Fig 3B).
245 Interestingly, confocal microscopy analyses revealed more features of the infection
246 phenotype: while virulent strains from cluster 1 and 2 colonized the epithelia as large
247 aggregates/biofilm structures, less virulent strains from cluster 3 and 4 infected as single
248 colonies or small bacterial aggregates (Fig 3C and Fig S6). Virulent strains caused cell shredding
249 from the apical side of the epithelia and were found within the epithelial layer as shown by
250 the PA14 strain (Fig 3C). However, variation in colonization phenotype was observed within

251 each cluster (Fig S6), which could be attributable to the genetic background of each strain.
252 Interestingly, DK01_I and DK02_I strains from cluster 4 were the only bacteria targeting
253 mucus-producing cells (as shown by bacteria overlapping with MUC5AC+ cells) (Fig 3C and Fig
254 S6).
255

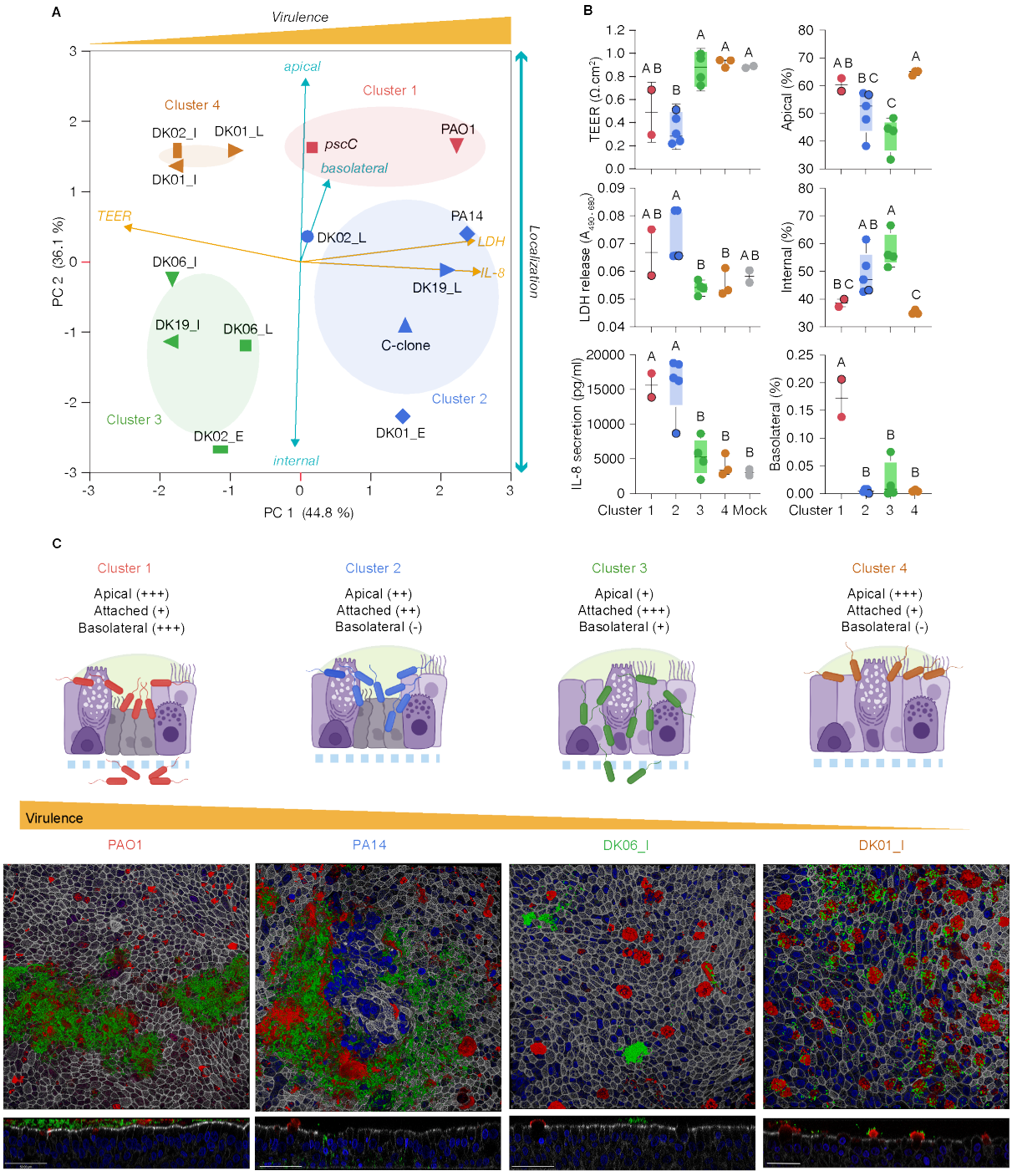

256

257 **Fig 3. Infection phenotypes of *Pseudomonas aeruginosa* strains.** A) PCA and K-mean
258 clustering of the infection phenotypes of laboratory (PAO1, *pscC*, PA14 and C-clone) and

clinical strains (early, intermediate, and late DK01, DK02, DK06 and DK19) of *P. aeruginosa.* Each symbol represents the median infection phenotypes in BCi-NS1.1, non-CF and CF cultures explained by the variables TEER, LDH release, IL-8 secretion, and distribution of bacteria in the apical, attached, and basolateral compartment. K-mean clusters (1 to 4) and PCA loadings are colour-coded to underline groupings of strains and explained variance, respectively. B) Box plot of the specific K-mean clusters characteristics for TEER, LDH release, IL-8 secretion, and normalized distribution of CFUs in the apical, attached and basolateral compartment. The outlined symbols in clusters 1 and 2 represent strains *pscC* and DK02_L, respectively. Statistical significance was computed by Kruskal-Wallis followed by Dunn's post-hoc test, connecting letters report significance between groups ($p<0.05$). C) Colonization phenotype of strain-specific clusters in CF cells. Schematic representation of ALI-CF epitheliums (purple) challenged with strains from clusters 1 (red), 2 (blue), 3 (green), and 4 (brown). Representative confocal microscopy images of CF-ALI cultures infected with strains from Cluster 1 (PAO1), Cluster 2 (PA14), Cluster 3 (DK06_I) and Cluster 4 (DK01_I). Top and side views of transwells are shown. Representative images from all strains infecting CF-ALI cultures are shown in Fig S6. Immunofluorescence staining: sGFP (green) staining chromosomally tagged bacteria; MUC5AC (red) specific for mucus producing cells; Phalloidin (white) specific for actin and DAPI (blue) nuclear stain. Staining's were done in three biological replicates, one representative image is shown for each infection. PCA: principal component analysis; TEER: transepithelial electrical resistance; LDH: lactate dehydrogenase; IL-8: interleukin 8.

Dual RNA-sequencing of P. aeruginosa *infecting ALI cell cultures*

While different bacterial strains showed similar infection patterns regardless of the infected ALI culture, the molecular responses of both the bacteria and the host might be strongly influenced by the specific cell culture and bacterial strain combination. To test this hypothesis, we performed dual RNA-seq experiments of ALI cultures from a CF and a non-CF donor and the BCi-NS1.1 cell line, infected with PAO1, *pscC* strain and mock (Fig 4A, Table S2: RNAseq). This approach allowed us to analyze the molecular response of bacteria with a clean background, eliminating the variable of the historical contingency of clinical strains, while still capturing the colonization process of highly virulent (PAO1) and intermediate virulent-like (*pscC*) clinical strains (Fig 3A).

PCA analysis of the host expression response (18746 genes, Fig 4B) showed that: 1) the transcriptional program of host-infected tissues (ALI-PAO1 and ALI-*pscC*) differed from that of non-infected cultures (ALI-mock) on PC 1 (Fig 4B), and 2) primary cells (non-CF and CF) exhibited different host responses relative to the BCi-NS1.1 cell line on PC 2 (Fig 4B). Meanwhile, the analysis of the bacterial expression profiles (4255 genes, Fig 4C) revealed subclusters based on: 1) the ALI model with non-CF and BCi-NS1.1 colocalizing on PC 1 (Fig 4C), and 2) the bacterial genetic background (top *pscC*, bottom PAO1) on PC 2 (Fig 4C). Bacteria colonizing non-CF and the BCi-NS1.1 ALI models showed almost identical gene expression profiles independently of the strain used (PAO1 or *pscC*), while growth on CF airway tissue seemed to drive a distinct bacterial expression profile. As a control and to validate our RNA-seq experiment, we correlated the IL-8 secretion during the infection with its corresponding gene (CXCL8) expression (Fig 4D), which showed a positive and significant correlation (Pearson's r= 0.9891; p < 0.0001). This confirms that infected samples have higher cytokine levels compared to the mock indicating ongoing inflammation.

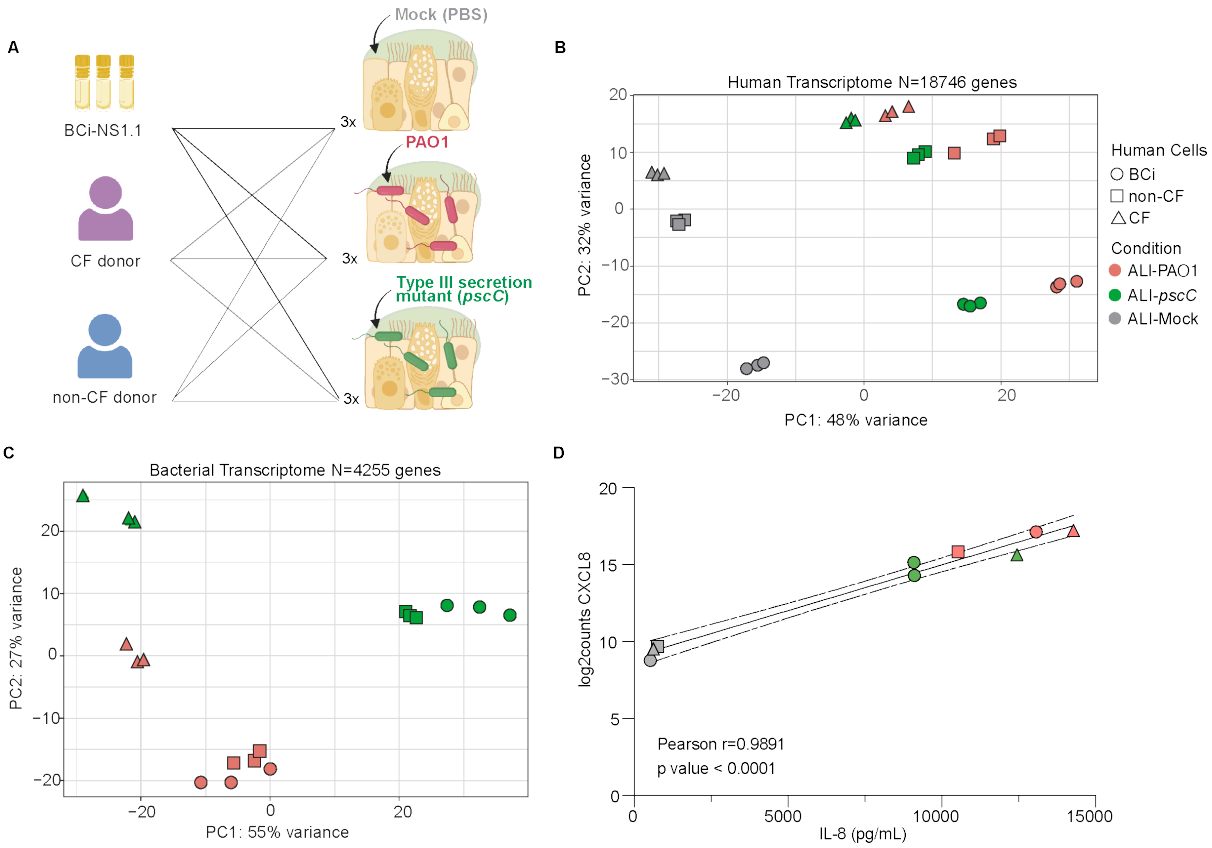

Fig 4. Exploring the transcriptional responses from human and pathogen upon co-culture. A) Schematic representation of the ALI cultures, host tissues (CF, purple; non-CF, blue; BCi-

308 NS1.1, yellow) and bacteria (PAO1, red; *pscC*, green) used to perform infections and
309 subsequent dual-RNAseq. RNA was extracted from three (3x) biological replicates. PCA of log_2
310 read counts from B) the host and C) the pathogen. Data included the reads of 18746 genes
311 from the human transcriptome and 4255 from the *Pseudomonas aeruginosa* transcriptome,
312 from which differential gene expression analysis was performed. Human tissues are presented
313 by symbol shapes: BCi-NS1.1 (circle), CF (triangle) and non-CF (square). Non infected (mock)
314 cultures are colored in grey, whereas ALI cultures with PAO1 or *pscC* are shown in red and
315 green, respectively. Each dot represents one biological replicate. D) Regression lines and
316 Pearson correlation coefficient for IL-8 quantification and the gene expression (log_2 read
317 counts). 95% confidence interval lines for the linear regression fit are included. ALI: air-liquid
318 interface; CF: cystic fibrosis; PCA: Principal component analysis; TEER: transepithelial electrical
319 resistance; IL-8: interleukin 8.
320
321 *Cellular and inflammatory responses in ALI cultures upon infection with PAO1 and* pscC
322 To characterize the molecular basis of the host response with either PAO1 or *pscC*, we
323 performed individual differentially expressed genes (DEG) comparisons between a) PAO1-
324 infected and mock cultures (Fig 5A), and b) PAO1-infected and *pscC*-infected cells (Fig 5D). For
325 each comparison, we first compared gene convergence/divergence across the different cell
326 types and second, we performed gene set enrichment analysis using both KEGG and the
327 MSigDB (GO) database (refer to Materials and Methods).
328 Compared to mock, CF cultures infected with PAO1 had the fewest DEG, followed by
329 non-CF and BCi-NS1.1 cultures which showed the highest number of DEG. For all CF, non-CF,
330 and BCi-NS1.1 infected samples, we observed mainly upregulated genes (Fig 5B, Table S3).
331 Enrichment analysis showed that *P. aeruginosa* triggers the upregulation of several pathways
332 related to inflammation via NF-kß and TNFα and overexpression of cytokines, including IL-6
333 and IL-17 signaling (Table S4). Of note, colony-stimulating factor CSF3 and pro-inflammatory
334 cytokine IL17C were among the most DEG across all host cells (mean log_2 FoldChange = 12.01
335 ± 1.5 and 11.8 ± 0.6, respectively) (Fig 5C). Other highly expressed genes include chemokine
336 ligand 20 (CCL20) and tumor necrosis factor (TNF), Toll-like Receptor (TLR)-2, TLR4 (involved
337 in recognition of bacterial pili or LPS), IL1B, IL6, CXCL8 (involved in first stages of infection) and
338 DEF4BA with antimicrobial capabilities (Fig 5C).

339 We found that the host responses after infection with the less virulent strain *pscC*
340 showed limited differences compared to PAO1 infection. In fact, only 65 unique genes were
341 differentially expressed (upregulated) in tissues infected with PAO1 relative to *pscC* (Fig 5E).
342 Pathways related to cytokine signaling and immune system response were overrepresented
343 among the set of genes with the highest expression in PAO1-infected non-CF and BCi-NS1.1
344 cultures (Fig 5F). This suggests that, at the time tested, the delivery of effectors from the T3SS
345 partially affects host cell gene expression. However, *P. aeruginosa* has a wide array of other
346 host-related virulence factors contributing to infection and concomitant inflammatory
347 response, possibly explaining the limited difference between the PAO1 and *pscC* mutant
348 strain.
349

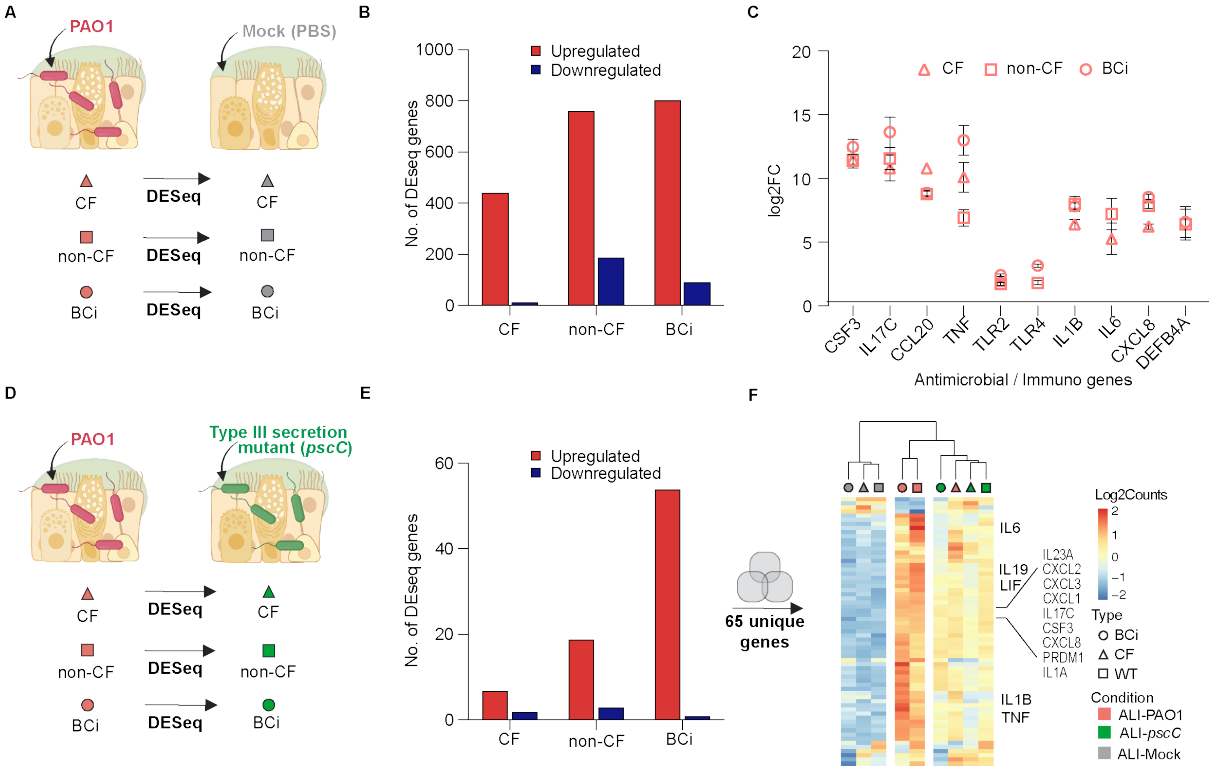

350

351 **Fig 5. Intrinsic host responses before and after colonization with PAO1.** A) Representation of
352 the individual differential expression (DE) comparisons between cultures were performed:
353 PAO1 infected cultures and their mock. B) Number of differentially expressed genes (DEG)
354 shown as upregulated (red) and downregulated (blue). An adj p value < 0.05 and
355 $\log_2$FoldChange > |1| was used as cutoff C) $\log_2$FoldChange of immune genes when comparing
356 PAO1 infected and mock. Only significantly expressed DEG are shown. D) Representation of
357 the DEG comparisons between PAO1-infected and *pscC*-infected cultures. E) Number of DEG

358 shown as upregulated (red) and downregulated (blue). F) Heatmap of log_2 read counts scaled
359 for each gene (row) from the unique 65 DE genes from D). Each column represents the mean
360 of the three biological replicates sequenced clustered based on the result of pvclust analysis.
361 CF: cystic fibrosis; BCi: BCi-NS1.1.
362
363 P. aeruginosa *PAO1 and* pscC *elicit differential response upon interaction with human airway*
364 *epithelial cells*
365 The analysis of the bacterial transcriptome aimed to evaluate how the expression profile of
366 PAO1 and *pscC* vary when interacting with different cell types (Fig 6A). As previously shown in
367 Fig 4C, whole-gene expression profile of both bacteria was similar in the non-CF and BCi-NS1.1
368 models. Indeed, no PAO1 gene was DE when comparing non-CF vs BCi-NS1.1 infections, and a
369 similar observation was obtained for *pscC* with only 3 DEG (Fig 6B top and bottom panel, Table
370 S5). The PAO1 transcriptome showed only 56 and 79 (total analyzed transcriptome n = 4255
371 genes) DEG in CF vs non-CF and CF vs BCi-NS1.1 infections, respectively, suggesting that PAO1
372 behaves rather similarly when colonizing different ALI cultures (Fig 6B). In contrast, *pscC* strain
373 showed a 3.9-fold to 5-fold increase in DEG in the CF vs non-CF and CF vs BCi-NS1.1
374 comparisons, respectively (Fig 6B, bottom panel). This suggests that the activity of T3SS has a
375 direct effect on bacterial expression profile upon infection with CF cultures.
376 Considering similarities between bacterial gene expression in non-CF and BCi-NS1.1
377 ALI models, we next focused on the CF vs non-CF comparison and compared the expression
378 profiles of *pscC* and PAO1 (Fig 6B underlined boxes). Deletion of T3SS *pscC* gene elicited a
379 much higher dysregulation of genes (up- or downregulated) when infecting CF ALI cultures
380 (unique DEG = 232, PAO1 specific n= 14, *pscC* specific = 177) (Fig 6B). From the total unique
381 DEG (n = 232), 41 were common to both strains and included upregulation of genes involved
382 in respiration under iron-limiting conditions such as 1) bo_3 quinol oxidase (*cyo*) genes and 2)
383 members of the *fumC-sodM* iron-responsive operon [41,42] (Table S6). Likewise, they both
384 downregulate several pathways reported as involved in virulence, such as the production and
385 transport of phenazines (among others: *phz1* and *phz2* operons), nitrate reductase *nirA,* and
386 fucose-specific lectin *lecB* [43–45].
387 When comparing CF vs non-CF infections for *pscC*, we found enrichment (upregulated)
388 of mainly 3 categories of genes: 1) iron chelation (related to heme uptake, pyoverdine, and
389 pyochelin transport), 2) sulfate metabolism (*cysAWT-sbp* operon), and 3) lipid A modifications

390 (Fig 6C, left panel and Table S6). Contrarily, several genes related to virulence including QS and
391 biofilm pathways, were enriched in the downregulated class (Fig 6C, right panel and Table S6).
392 For example: 1) genes from the *pseudomonas* quinolone signal (PQS) cluster, 2) rhamnolipids
393 coding genes, 3) the type 6 secretion system H2 gene cluster (H2-T6SS), 4) genes from oxide-
394 sensing mechanisms, and 5) elastases (*lasB*) and pyocyanin biosynthetic genes. This suggests
395 that upon CF infections, *P. aeruginosa* regulates several pathways involved in iron starvation,
396 respiration, and virulence mechanisms which were previously identified as differentially
397 expressed *in vivo* in CF airways and contribute to the establishment of the infection [46,47].
398

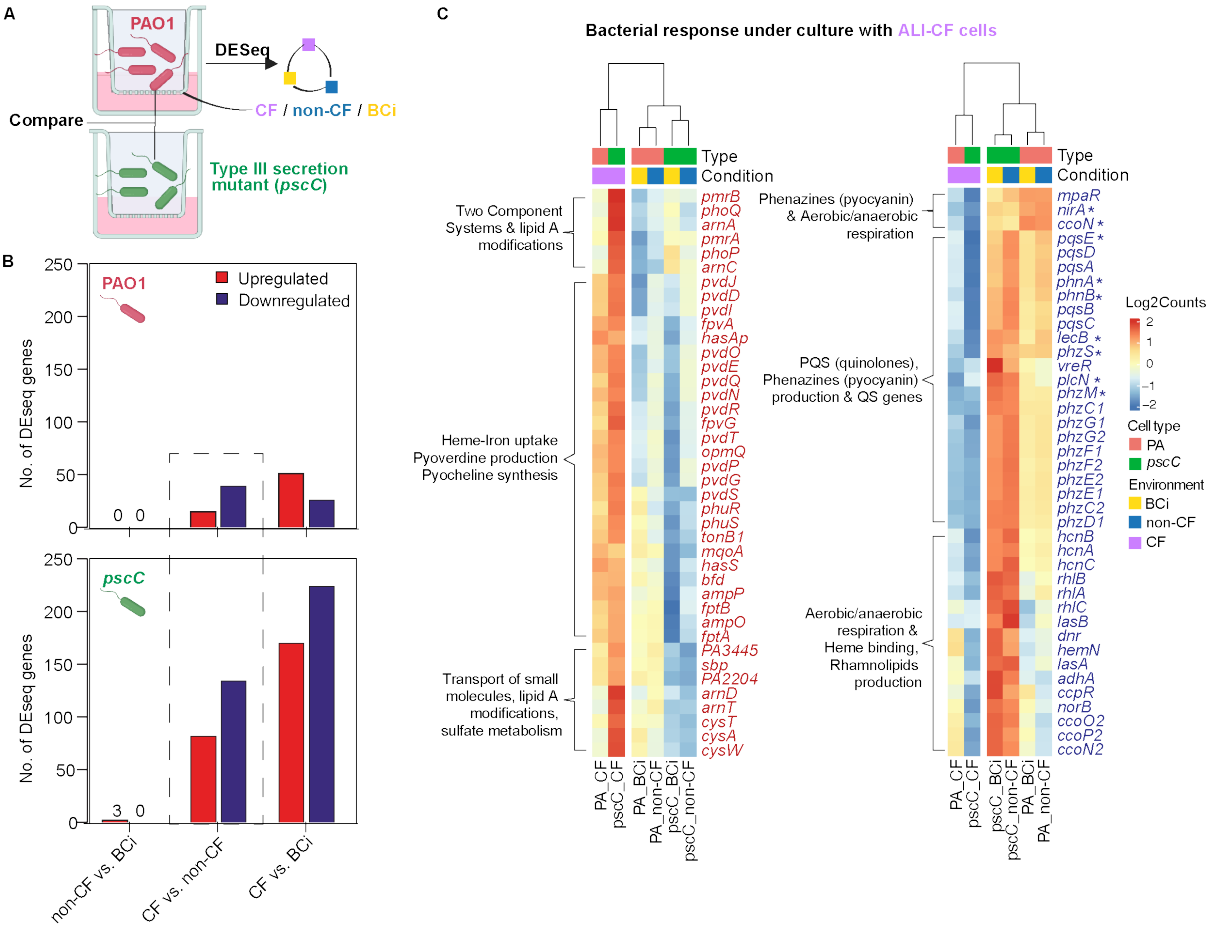

399

400 **Figure 6. *Pseudomonas aeruginosa* responses upon interaction with different human cell**
401 **types.** A) Representation of the differentially expressed gene (DEG) comparison of PAO1 and
402 *pscC* transcriptomes analyzed in different ALI models, ie. non-CF vs. BCi, CF vs. non-CF, and CF.
403 vs BCi. B) Number of DEG shown as upregulated (red) or downregulated (blue) and separated
404 by strain (PAO1 top and *pscC* bottom panel, respectively). An adj p value < 0.05 and
405 $\log_2$FoldChange > |1| was used as cutoff. C) Heatmap of $\log_2$ read counts scaled for each gene

406 (row) present in selected categories from Table S6, comparison *pscC* CF vs. non-CF. Each
407 column represents the mean of the three biological replicates sequenced, clustered based on
408 the result of pvclust analysis. Genes with asterisk (*) were differentially expressed (DE) in both
409 PAO1 and *pscC* strains when comparing CF vs. non-CF models. CF: cystic fibrosis; BCi: BCi-
410 NS1.1.
411
412
413 **Discussion**
414 Persistent bacterial infections are often associated with antibiotic resistance, but several other
415 underlying mechanisms have been brought forward to explain why antibiotic treatment fails
416 to eradicate the infecting bacteria. Thus, eradication failure of *P. aeruginosa* in pwCF requires
417 the understanding of the infection and colonization process and the interactions between the
418 host and the pathogen. For this, we have established and compared infection model systems
419 based on ALI cultures of different human airway epithelial cells (non-CF, CF and the BCi-NS1.1
420 cell line), in which we have quantified infection outcomes during the early stages of
421 colonization by different clinical isolates of *P. aeruginosa*.
422 In a first physiological response investigation of the differentiated airway epithelial ALI
423 cultures, we quantified a number of tissue parameters after the bacterial colonization:
424 epithelial damage (transepithelial electric resistance, TEER), cytotoxicity (release of lactate
425 dehydrogenase, LDH), immune system recruitment (interleukin 8), and bacterial distribution
426 in the tissue (confocal microscopy). Together, the patterns of changes of these 4 parameters
427 provide highly valuable information about the inherent properties of the included tissues, as
428 well as about the virulence of the infecting bacteria. Thus, our investigations revealed that
429 irrespective of the host tissues (non-CF and CF donors or the BCi-NS1.1 cell line), colonization
430 of different epithelia was predominantly driven by the intrinsic bacterial virulence potential.
431 Infection clusters were neither based on the strain's genetic background (that is, isolates from
432 the same lineage were not always grouped together), nor on the level of adaptation (that is,
433 chronic late strains did not always show reduced virulence). Yet, several studies of clinical
434 strains grown *in vitro* have revealed convergence in different lineages to an adapted and low
435 virulent phenotype as chronic infection progresses [21,24,36,37]. However, transcriptomic and
436 proteomic changes do not always positively correlate with *in vivo* data due to differences in
437 growth conditions and the lack of host interactions [46,47]. Importantly, the ALI system used in

438 this study has the potential to become a powerful infection predictive method, as it allows the
439 evaluation of drug efficacy, immune system activity, host responses, and inter-species
440 interactions, which are fundamental to understanding infection progression and improving
441 treatment outcomes. Recently, certain mutations in *P. aeruginosa* were discovered to be
442 involved in novel adaptive mechanisms that transcend conventional antibiotic resistance,
443 which highlights the need for host-focused approaches to develop more effective strategies
444 for managing bacterial infections [29,30]. Interestingly, in our ALI model system using CF cultures,
445 we observed similar infection profiles of both laboratory and clinical strains of *P. aeruginosa*,
446 whether treated with ETI modulators or not. This is in agreement with recent works showing
447 that, albeit there is a reduction of bacterial load in pwCF treated with ETI modulator, bacteria
448 still persist in the airway [9,11].

449 Interactions of *P. aeruginosa* with airway epithelial cells grown in ALI systems have
450 recently been investigated by transcriptomic analyses to study the pathogen, the host, or both
451 [31,33,34,48,49]. Given the system's complexity and the technical challenges of working with
452 primary cells ALI infections, we only explored the gene expression response of PAO1 and the
453 less virulent *pscC* strain when infecting ALI models from a CF and a non-CF donor together
454 with the BCi-NS1.1 cell line. Although we cannot rule out differences in gene expression
455 between donors, our ALI infections and non-RNA readouts were carried out with several
456 donors, where infection patterns were evened out. Similar to earlier research, we found that
457 colonization of host epithelium with *P. aeruginosa* triggers the upregulation of NF-kß and
458 TNFα pathways and overexpression of cytokines including those coding for IL-6 and IL-17
459 signaling [33,34,49]. Moreover, our three ALI models shared the same profile with 368 common
460 DE genes related to bacterial infection response such as inflammatory pathways, response to
461 bacteria and LPS. In agreement with the latter, infections carried out with 8 different donors
462 (n = 3, non-CF and n = 5, CF) showed similar trends in IL-8 secretion for PAO1 across the
463 different cell types. On the other hand, like PAO1, deletion of T3SS also induced host
464 inflammation, and only 65 genes related to cytokines and immune markers (e.g. CSF3, IL1B,
465 IL6, CXCL8 and TNF) were upregulated during PAO1 infection while they were significantly
466 downregulated during the *pscC* infection when comparing PAO1 vs *pscC* infected samples (Fig
467 5F and Table S5). This correlates well with infection readouts, in which *pscC* strain still showed
468 an intermediate virulence potential between PAO1 and the more adapted clinical strains (Fig
469 3).

470 Upon infection and depending on the availability of nutrients and/or signals triggered
471 by host cells, *P. aeruginosa* tightly controls the regulation of a wide array of virulence factors
472 involved in host-mediated respiratory infections [26]. In our CF model, both PAO1 and *pscC* strain
473 limit the expression of *lasB*, a principal extracellular virulence factor, and the biosynthesis of
474 pyocyanin, both contributing to inflammation and epithelial disruption [50]. The downregulation
475 of these genes may enable the bacteria to evade the host's immune system and reduce host
476 inflammation, as observed in our infected CF models, which showed fewer DEG (n = 442)
477 compared to the non-CF (n = 761) and BCi-NS1.1 (n = 804). Strikingly, the response between
478 CF cells and the T3SS-deficient *pscC* strain showed a much more complex dysregulation
479 resembling many of the features already seen in CF clinical isolates. This suggests that CF
480 models would be the best suitable approach when the research focus is on bacterial
481 transcription. Besides phenazine biosynthesis, the *pscC* strain also shows a downregulation of
482 the PQS system and rhamnolipid production, mirroring key features of CF late chronic strains
483 [46]. Another example is the high expression of genes involved in the production and
484 transportation of siderophores pyoverdine (*pvd*) and pyochelin (*pch*), as well as the
485 assimilation of heme (*phu* and *has* systems) [47], which suggests that the accessibility of these
486 micronutrients is limited in CF ALI models relative to non-CF.
487 While infection model systems allow for a more representative analysis of bacterial
488 phenotypes, they also have some limitations. It was, indeed, surprising that only a few isolates
489 showed significant differences in one or two readouts between CF and non-CF cultures. This
490 result may be due to several factors: a) the model may not accurately reflect the conditions
491 bacteria encounter in the lung (i.e., presence of immune cells, antibiotic treatment, oxygen
492 and micronutrient gradients), b) the length of infection (14 or 38 h) might be sub-optimal for
493 discriminating small infection pattern responses, c) the closed nature of the ALI transwells
494 which limits mucociliary clearance and mucus buildup, potentially making the different cell
495 types similar, or d) the lack of residing airway microbiota which could influence the host-
496 pathogen interaction. Therefore, further investigations are required to evaluate each
497 parameter.
498 Altogether, we explored the virulence potential of persistent clones of *P. aeruginosa*
499 when colonizing different airway epithelial tissues grown at the ALI interface. We covered a
500 variety of bacterial lineages and host donors and defined clusters of infection properties.
501 Furthermore, we quantified the transcriptional responses of both pathogen and host upon

infection at a whole population level. Our data foster the need for studies using host-pathogen models to recapitulate the *in vivo* conditions of pathogenic diseases. Moreover, given the more appropriate physiological environment, it serves as a platform for evaluating treatment efficacy and identifying novel therapies for the treatment of persistent infections. Still, further studies including immune cells, antibiotic treatment, and other infecting species are needed to understanding infection progression, antibiotic treatment failure and new mechanisms of persistence.

511 **Materials and Methods**

512 **Primary human airway cells and cell line used**

513 Nasal brushing, nasal polyps and distal lung biopsies were obtained from pwCF (n = 10) and
514 non-CF control (n = 5) donors. Details of CFTR mutation and sample usage are provided in
515 Table S2. Nasal brushes were obtained using a 2.5mm sterile cytology brush and placed in
516 Dulbecco´s modified essential media (DMEM) supplemented with primocin (1 mg/mL),
517 gentamicin (100 µg/mL) and Amphotericin B (2.5 µg/mL) until further processing for cell
518 culture. Polyps were obtained from patients undergoing endoscopic sinus surgery. Tissue
519 specimens were surgically removed and immediately placed in DMEM supplemented with
520 same antibiotics as brush biopsies. Size of explants obtained was of approximately 20–30
521 mm^2. Explants were washed three times with fresh, sterile media, to remove blood and
522 mucous when was present.

523 Isolated basal cells were seeded and expanded in T-25 cm^2 flasks (corning Life Sciences)
524 previously coated with human type I collagen (Gibco, A1048301) in a 37°C, 5% CO2 humidified
525 incubator, using Pneumacult-Ex Plus medium (STEMCELL Technologies, 05040) supplemented
526 with Pneumacult-Ex 50x supplement (STEMCELL Technologies, 05008), 96 ng/mL
527 hydrocortisone (STEMCELL Technologies, 07925), 10 µM Y-27632 ROCK inhibitor (Bio-Techne
528 #1254/10), and the same antibiotics used before. Following expansion, 1.5 x 10^5 cells were
529 seeded onto 6.5-diameter-size transwells with 0.4 µm pore polyester membrane insert
530 (Corning Life Sciences) previously coated with type I collagen.

531 Once cells reached full confluency, Air-Liquid Interface (ALI) was established, by removing
532 media from the apical chamber and replacing media in the basolateral chamber with
533 Pneumacult-ALI medium (STEMCELL Technologies) supplemented with 480 ng/mL
534 hydrocortisone (STEMCELL Technologies), 4 µg/mL heparin (STEMCELL Technologies, 07980),
535 Pneumacult-ALI 10x supplement (STEMCELL Technologies) and Pneumacult-ALI maintenance
536 supplement (STEMCELL Technologies). ALI cultures were grown at 37 °C and 5% CO_2 in a
537 humidified incubator for 28 days, with media replacement twice a week.

538 Epithelial polarization was monitored by measurements of the transepithelial electrical
539 resistance (TEER) using an EVOM2 (World Precision Instruments) and a chopstick electrode
540 (STX2; World Precision Instruments). Following 15 days under ALI conditions, the apical
541 surface was washed with 1x Phosphate Buffered Saline (PBS) once a week to remove
542 accumulated mucus. For primary cells only passage 1-3 were used for ALI cultures. Different

543 studies have show that both human nasal and bronchial airway epithelial cells grown for ALI
544 cultures are representative of lung biology and recreate its physiology [28,51].
545 The Basal Cell Immortalized Non-Smoker 1.1 (BCi-NS1.1) cell line [35] was used for comparison
546 with the primary ALI infection model systems. BCi-NS1.1 cell expansion, ALI establishment,
547 differentiation and maintenance of cell cultures was performed as described above for
548 primary cells without the addition of antibiotic to media culturing.
549
550 **Modulator treatment**
551 On day 28, a combined CFTR-modulator treatment of elexacaftor (VX-445, MedChemExpress),
552 tezacaftor (VX-661, Selleck Chemicals LLC) and ivacaftor (VX-770, Selleck Chemicals LLC), was
553 added for 24h to the basolateral medium, with a final concentration of 3 µM, 10 µM and 5
554 µM in 0.15% dimethyl sulfoxide (DSMO), respectively. The treatment was prepared fresh
555 before each experiment. Controls were treated with similar concentration of DSMO.
556
557 **Measurement of CFTR function and rescue**
558 Transepithelial electrical conductance (TEEC) is considered a parameter to assess the CFTR
559 function, as demonstrated in previous studies [52–54]. TEEC is calculated from the reciprocal
560 value of TEER measurements:

561 $$Transepithelial\ electrical\ conductance(TEEC) = \frac{1}{Resistance} = \frac{1}{TEER}$$

562 $$\Delta TEEC = TEEC(\max) - TEEC(inhib)$$

563
564 The rescue of CFTR function through ETI treatment facilitates the transepithelial chloride ion
565 transport, and increases the CFTR-dependent TEEC.
566 TEER measurements were obtained after maximal stimulation of CFTR channels with forskolin
567 plus genistein and subsequent inhibition with PPQ-102, before converted to TEEC. The
568 difference between maximum activation and inhibition (ΔTEEC) reflects the CFTR activity in
569 the epithelia, and the difference between treated and un-treated cells reflects the partial
570 rescue of CFTR function by ETI. First, Coon's modified Ham's F12 medium (DiagnoCine), where
571 NaHCO3 was replaced with 20 mM Na-Hepes (SigmaAldrich) (pH 7.3), was added to both sides
572 of the cell layer, and after one hour of equilibration, a baseline TEER was measured in each
573 transwell as described previously (workflow is shown in Figure S2). After 10 minutes, apical

574 amiloride was added to block sodium channels (ENaCs), and to avoid sodium-dependent
575 currents. Apical and basolateral medium was replaced with new solutions containing forskolin
576 10 µM (TargetMol) and genistein 50 µM (TargetMol) activate CFTR function. To subsequently
577 inhibit CFTR function, a solution containing CFTR inhibitor PPQ-102 30 µM (TargetMol) was
578 added to the apical side. Between each step, a 10 min incubation time was allowed, after
579 which TEER was measured and values were subsequently converted to TEEC. All donors, CF
580 and non-CF, were tested to assess the ETI response, in at least three technical replicates.
581 Following test of CFTR function, the cell cultures were discarded, and were not utilized in
582 subsequent infection experiments.
583
584 **Clinical strains, growth conditions and fluorescent tagging**
585 Strains used in this study are summarized in Table S1. Clinical strains were obtained from
586 sputum samples from pwCF attending or who have attended the Copenhagen Cystic Fibrosis
587 Center at University Hospital Rigshospitalet, Copenhagen, Denmark. Sputum sampling is a
588 part of the routinary visits to the CF clinic and was not performed for the purpose of this
589 research. All clinical strains except for DK01_E, DK02_E, were previously sequenced and their
590 genomic and transcriptomic profile was characterized [36].
591 *P. aeruginosa* reference strains PAO1, PA14 and C-clone were obtained from the Leibniz
592 Institute DSMZ collection with references DSM22644, DSM19882 and DSM29238,
593 respectively. Additionally, an isogenic mutant of PAO1, encoding the *pscC* gene, part of the
594 T3SS, was constructed in the lab.
595 All strains were tagged with a superior green fluorescent protein (sfGFP) to enable
596 visualization by confocal microscopy. Bacterial strains were GFP-tagged by 4 parental mating
597 using the miniTn7 delivery plasmid with rhaSR-PrhaBAD inducible promoter (pJM220) [55].
598 Plasmid was engineered in the lab to accommodate sfGFP gene. Transformants were selected
599 on *Pseudomonas* isolation agar supplemented with Gentamicin 30 µg/mL. The final sfGFP-
600 tagged strains were verified by checking green fluorescence using a Leica DM4000 B
601 epifluorescence microscope and confirming normal growth rate (Fig S7).
602
603 **Phenotypic characterization of *P. aeruginosa* strains**
604 Strains were characterized based on their growth in synthetic cystic fibrosis media (SCFM),
605 bacterial movement and antibiotic susceptibility profiles. Briefly, single colonies were picked

606 and grown on liquid Luria-Bertani broth (LB) cultures. Cultures were standardized to OD = 0.1
607 and further diluted to OD = 0.01 in SCFM media and growth was recorded every 15 min for 18
608 h in a 96 well plate reader at 37°C with continuous shaking. Doubling times and growth rate
609 estimations were calculated using Graph Pad Prism software (v 10.2.2), focusing on the
610 exponential part of the growth curve. For swimming assay, 2 µl of the 0.1 OD cultures were
611 plated on the center of tryptone broth plates (10 g/L tryptone, 5 g/L NaCl) with 0.25 % of
612 agarose. Motility diameter was measured after incubation for 6 h at 37°C and additional 16 h
613 at room temperature. For antimicrobial susceptibility, the microdilution method from EUCAST
614 was used (The European Committee on Antimicrobial Susceptibility Testing 2023). Cultures
615 were standardized to Mc Farland (5 x 10^5 CFU/ml) and grown in Müller-Hinton broth with
616 serial fold dilutions of either tobramycin, ceftazidime, or ciprofloxacin for 16 h in 96 well plates
617 at 37 °C with shaking conditions. MIC was calculated as the concentration of antimicrobial that
618 completely inhibited the growth of the strain as detected by the naked eye. All phenotypic
619 experiments were performed with 3 independent cultures.
620
621 **Infection of ALI cultures with *P. aeruginosa* strains**
622 Overnight of *P. aeruginosa* cultures were standardized to OD = 0.05 (fast growers) – 0.1 (slow
623 growers) and grown until mid-exponential phase in 5 mL of LB medium. Subsequently, 1 mL
624 of culture was centrifuged at 5000 × g for 5 min, and bacterial pellets were washed with PBS
625 and resuspended in PBS at a concentration of 10^5 CFUs/mL. For each strain, the relationship
626 between OD and CFU count was tested in triplicates to achieve reproducible results. 10 µL
627 aliquot of this solution, containing 10^3 CFUs, was inoculated onto the apical side of fully
628 differentiated ALI cultures, each with 600 µL of supplemented Pneumacult-ALI maintenance
629 medium in the basolateral chamber. Non infected controls were inoculated with an equal
630 volume of bacteria-free PBS. Infected cells were incubated at 37 °C and 5% CO2 in a humidified
631 incubator for the specified duration required to characterize the infection (14 h for fast
632 growers and 38 h for slow growers). Following infection time, 200 µL of PBS was added to the
633 apical side, and TEER was measured.
634 Subsequently, the 200 µL of PBS from the apical side and 600 µL of medium from the
635 basolateral side were collected and CFUs present in these samples were quantified by plating
636 10 µL of serial dilutions on LB-agar plates. The remaining samples were preserved at −80 °C
637 for future analysis. For quantification of bacterial CFUs attached to the epithelium 200 µL of

638 0,01% triton in PBS was added to the apical part, and the epithelial layer was disrupted using
639 a cell scraper. CFUs present in the suspension were determined as explained above.
640
641 **Immunofluorescence staining and confocal microscopy**
642 ALI cultures were fixed with 4% paraformaldehyde added in both apical and basolateral
643 compartments for 20 min at 4 °C. After fixation, cells were washed 3 times with PBS after
644 which and incubation of 1 h at room temperature (RT) with blocking buffer (0.1% Triton X-100,
645 1% saponin, 3%BSA in PBS) was performed to allow permeabilization. Then, whole transwells
646 were stained overnight with a 100 µL solution of MUC5AC (mouse monoclonal, Invitrogen) at
647 1:100 dilution. For CFTR staining, a solution of anti-CFTR 570 at 1:100 dilution and incubated
648 overnight at 4°C was used. The following day, a second staining was performed with a new
649 100 µL aliquot containing Phalloidin-Alexa Fluor 555 (Invitrogen), DAPI (Thermo Scientific) and
650 Alexa Fluor 647 (Invitrogen) at 1:400, 1:750, 1:500 dilution, respectively. All stainings were
651 conducted in a buffer containing 3%BSA and 1% saponin in PBS. After staining the membranes
652 were removed from their supports with a scalpel and mounted on glass slides with
653 VECTASHIELD® Antifade Mounting Medium (VWR). Images were acquired with a Leica Stellaris
654 8 Confocal Microscope (40× magnification, 1.3 oil) and analyzed using the LasX software
655 1.4.4.26810 (Leica).
656
657 **Lactate dehydrogenase (LDH) release and Human IL-8 production**
658 Aliquots from basolateral compartment were further used for measuring LDH and IL-8 release
659 following the manufacturer's instructions of the Invitrogen™ CyQUANT™ LDH Cytotoxicity
660 Assay Kit (Invitrogen, C20301) and Human IL-8/CXCL8 DuoSet ELISA kit (Bio-Techne, DY208).
661 LDH was measured using 50 µL of media and measuring absorbance at 680 nm and 490 nm.
662 For IL-8 quantification, basolateral media was diluted to 1:10 and absorbance was measured
663 at 450nm and 540nm. All individual ALI infected samples were tested in triplicates.
664
665 **RNA extraction from ALI cultures and sequencing library preparation**
666 Lung biopsy from one wild-type donor (non-CF 16) and nasal brush from one pwCF (CF14) and
667 the BCi-NS1.1 cell line were used to perform infection models with PAO1 and *pscC* strains, in
668 triplicates. ALI models and infections were performed as for the rest of the infections in this

669 work. Compared to other donors, infection readouts were within the experimental variability
670 (Table S2).
671 Extraction of RNA was performed using the Qiagen RNeasy Plus Mini kit and following
672 manufacturing protocol. Briefly, after infection was performed and TEER was measured, PBS
673 media was removed from the top and 300ul of RNA protect Cell Reagent was added. Adherent
674 cells detached after thorough pipetting without need of trypsin. Two transwells were collected
675 within 300ul of sample and froze at -80 until RNA extraction. For enzymatic lysis, samples were
676 thawed and centrifuged to remove RNA protect, and then 1ml RNA-se free water containing
677 1 mg/ml of lysozyme was added and incubate for 30min at 37°C. Then samples were
678 centrifuged and resuspended in 600ul RLT Buffer (with ß-mercapto) and follow Qiagen
679 protocol to recover RNA fragments over 200 nt. Recovered RNA was quantified using
680 fluorimetric quantitation with Qubit® RNA BR Assay kit (Invitrogen) and RNA integrity was
681 measured on an Agilent Bioanalyzer 2100 machine (Agilent technologies) using a RNA Nano
682 kit. All samples had a percentage of RNA fragments > 200 nt (DV_{200}) ranging between 50%-
683 75% and were further processed. 2 µg of eluted RNA was treated with DNAse I (Invitrogen)
684 for 30min at 37°C in a final volume of 50µl. Further clean up with Qiagen columns was
685 performed by mixing 3 times RLT Buffer (without ß-mercapto), with 3 times 95-100% ethanol
686 and 1 time sample (50µl sample + 150µl RLT + 150µl EtOH). Following 2 wash steps with RPE,
687 RNA samples were resuspended in 20-25 µl RNA-se free water. 500 ng of RNA was used as
688 template to prepare sequencing libraries with Illumina Stranded Total RNA Prep with Ribo-
689 Zero Plus kit (Illumina). Sequencing was performed on an Illumina NextSeq 500 sequencer,
690 using a high output kit, generating a minimum of 30 million reads per sample (75 bp, single
691 end reads).
692 As it has been shown that bacterial transcripts represent only a fraction of total RNA within
693 host cells [56], we extracted RNA from two independent infected transwells and consider it as
694 one replica, so the total of infections per condition was 6, and only a max. of 12 samples were
695 pooled for sequencing run. This strategy enables an increased yield in the bacterial RNA in the
696 infected cultures ranging from 2.5M to 10M reads depending on the bacteria and cell type
697 (Fig S8, Table S7). For *pscC* infected samples (BCi-*pscC* 1-3, CF-*pscC* 2-3, non-CF-*pscC* 1-3) a
698 second round of sequencing was done to reach a minimum cutoff of 1M reads for
699 *Pseudomonas* genome. Table S7 contains the sequencing reads achieved for both runs (BCi-
700 *pscC* 1a and BCi-*pscC* 1b, etc.).

701
702 **Host-Microbe transcriptome analysis**

703 Sequencing reads were analyzed with our in-house pipeline updated for host-microbe samples
704 [57]. Briefly, low-quality bases and contaminant adapters were trimmed using Trimmomatic (v
705 0.35), discarding reads shorter than 35 nt. Reads were further processed using the SortMeRNA
706 tool (v 2.1) to remove reads generated from residual rRNA transcripts. High-quality human
707 and bacterial reads were separated in silico by mapping reads using the BWA aligner and MEM
708 algorithm against the human genome assembly GRCh38.p9 retrieved from the NCBI database.
709 Reads not mapping on the human genome were used as input for analyzing the
710 transcriptionally active *P. aeruginosa* population mapping against *P. aeruginosa* PAO1 genome
711 (NCBI: NC_002516.2) using BWA (0.7.15-r1140) aligner and MEM algorithm with default
712 parameters.

713

714 **Gene expression analysis**

715 For gene expression analysis, mapped reads deriving from host and *P. aeruginosa* were
716 counted using htseq-count (v 0.7.2). Count tables were then imported into R for differential
717 gene expression (DEG) analyses. Host read counts were pre-filtered based on >= 10 reads
718 counts per condition (sum of replicates), yielding a count data of 18746 genes. Then, counts
719 were normalized using variance stabilizing transformation (VST-normalization) on all samples
720 together in the R package DESEq2 (v 1.44.0) with option blind = TRUE [58]. A similar approach
721 was set for bacterial reads, counts were pre-filtered based on all replicate's samples having >=
722 10 reads, reaching a count data of 4255 *P. aeruginosa* genes. Normalized counts were used to
723 evaluate whole transcriptome similarities between replicates and conditions using principal
724 component analysis (PCA) and hierarchical clustering analysis (HCA). PCA was performed using
725 plotPCA() function and visualize with ggplot(). When needed, normalized counts of specific
726 set of genes were visualized as heatmaps using pheatmap() function calculating first the
727 replicates mean in each condition.

728 To get list of log_2FoldChange values, from the initial DESeq2 result table, pair comparisons of
729 specific conditions were extracted using the "contrast" argument from the result() function in
730 DESeq2. For both host and bacteria, DEG were considered statistically significant when
731 log_2FoldChange ≥ |1.0| and an adjusted p value ≤0.05. Significant host DEG were used as input
732 for inspection of gene set enrichment analyses which considers both gene name and

733 log_2FoldChange values. The "human hallmark set" collection from Molecular Signature
734 Database (MsigDB) which is a non-redudant curated gene set based on GO terms pathways,
735 maintained by the GSEA team (www.msigdb.org) was used in R using functions msigdbr() to
736 call the gene set, and GSEA() for enrichment purposes, with the following parameters:
737 minGSSize=5, maxGSSize=500, pvalueCutoff=0.05, pAdjustMethod=BH. Functional
738 enrichment with the KEGG database using gseKEGG() function, was also performed. Here
739 terms were filtered based on pathway correlation with our infection model. When similar
740 pathways were called (response to lipid vs cellular response to lipid), the one with the smallest
741 padj value was used. Similarly, functional class enrichment in significant bacteria DEG was
742 performed using log2FoldChange values and gene associations with terms present in COGs
743 and KEGG classification databases, using PAO1 annotations from Pseudomonas.com and using
744 it as terms for GSEA(). For gseKEGG() the following parameters were used: organism="pae",
745 minGSSize=5, maxGSSize=500, pvalueCutoff=0.05, pAdjustMethod=BH.
746 To identify similarities across different DEG lists, UpSet plots were drawn using the UpSet()
747 function from R.
748
749 **Ethical approval and consent to participate**
750 This study was approved by the local ethics committee of the Capital Region of Denmark
751 (Region Hovedstaden), registration number H-20024750. All patients provided informed
752 consent to participate in the study and for the publication of associated results and pertinent
753 clinical data. Pseudonymization of patient information was performed to sever any links that
754 could lead to patient identification.
755
756 **Data sharing**
757 Raw sequence data supporting the results of this work are available as SRA BioProject under
758 Accesion No. PRJNA1153754 and accession numbers from individual BioSamples and
759 sequences is summarized in Table S7.
760
761 **Author Contribution Statement**
762 **Claudia Antonella Colque:** Methodology, Formal analysis, Investigation, Data curation,
763 Visualization, Writing – original draft, Writing – review & editing. **Signe Lolle:** Methodology,
764 Formal analysis, Investigation, Writing – review & editing. **Ruggero La Rosa:** Formal analysis,

Data curation, Visualization, Writing – original draft, Writing – review & editing. **Maria Pals Bendixen:** Investigation, Writing – review & editing. **Filipa Bica Simões:** Methodology, Formal analysis, Investigation, Writing – original draft, Writing – review & editing. **Kasper Aanæs**: Resources. **Søren Molin:** Conceptualization, Supervision, Writing – review & editing. **Helle Krogh Johansen:** Conceptualization, Funding acquisition, Resources, Supervision, Writing – review & editing.

Acknowledgments

The authors thank the Danish pwCF and the non-CF donors who participated in this study, Laura Elisabeth Bojesen Haapalo and Rene Horsleben Petersen (Department of Cardiothoracic Surgery, Copenhagen University Hospital, Rigshospitalet, Denmark) for providing and assisting with lung tissue samples, and the nurses from Rigshospitalet CF clinic assisting with patient recruitment and sample collection. We thank the cystic fibrosis foundation (CFF) for providing the CFTR anti570 antibody, and Ronald G. Cristal (Weil Cornell Medical College, New York, USA) for providing the BCi-NS1.1 cell line. This research was funded by a Challenge Grant (Ref. nr.: NNF19OC0056411) and a grant from The John and Birthe Meyer Foundation awarded to HKJ. HKJ and SM were supported by a grant from CAG. - Greater Copenhagen Health - Science – Partners (GCHSP), 2020. We thank the Infection Microbiology group (Asha Maria Rudjord Levann, Oihane Irazoqui Sanchez, Pablo Laborda Martínez, Janus Anders Juul Haagensen) for their insightful comments and discussions. We thank Elio Rossi (Department of Biosciences, University of Milan) for his advice on transcriptomics analysis, and Nicoletta Pedemonte from IRCCS Institute Gaslini, Genova for her assistance in modulator treatment assays.

References

1. La Rosa, R., Johansen, H. K. & Molin, S. Persistent Bacterial Infections, Antibiotic Treatment Failure, and Microbial Adaptive Evolution. *Antibiotics* **11**, 419 (2022).
2. Haney, E. F. & Hancock, R. E. W. Addressing Antibiotic Failure—Beyond Genetically Encoded Antimicrobial Resistance. *Front. Drug. Discov.* **2**, 892975 (2022).
3. Sheppard, D. N. & Welsh, M. J. Structure and Function of the CFTR Chloride Channel. *Physiological Reviews* **79**, S23–S45 (1999).
4. O'Sullivan, B. P. & Freedman, S. D. Cystic fibrosis. *The Lancet* **373**, 1891–1904 (2009).
5. Douglas, T. A. *et al.* Acquisition and eradication of P. aeruginosa in young children with cystic fibrosis. *European Respiratory Journal* **33**, 305–311 (2008).
6. Rosenfeld, M. *et al.* Diagnostic accuracy of oropharyngeal cultures in infants and young children with cystic fibrosis. *Pediatr. Pulmonol.* **28**, 321–328 (1999).
7. Heijerman, H. G. M. *et al.* Efficacy and safety of the elexacaftor plus tezacaftor plus ivacaftor combination regimen in people with cystic fibrosis homozygous for the F508del mutation: a double-blind, randomised, phase 3 trial. *The Lancet* **394**, 1940–1948 (2019).
8. Szabo, M. M. *et al.* Impact of elexacaftor/tezacaftor/ivacaftor on respiratory colonization in an adult cystic fibrosis clinic. *The American Journal of the Medical Sciences* **367**, 337–342 (2024).
9. Armbruster, C. R. *et al.* Persistence and evolution of *Pseudomonas aeruginosa* following initiation of highly effective modulator therapy in cystic fibrosis. *mBio* **15**, e00519-24 (2024).

10. Ledger, E. L. *et al.* Impact of CFTR Modulation on *Pseudomonas aeruginosa* Infection in People With Cystic Fibrosis. *The Journal of Infectious Diseases* **230**, e536–e547 (2024).
11. Nichols, D. P. *et al.* Pharmacologic improvement of CFTR function rapidly decreases sputum pathogen density, but lung infections generally persist. *Journal of Clinical Investigation* **133**, e167957 (2023).
12. Bartell, J. A. *et al.* Omics-based tracking of *Pseudomonas aeruginosa* persistence in "eradicated" cystic fibrosis patients. *Eur Respir J* **57**, 2000512 (2021).
13. Mésinèle, J. *et al.* Risk factors for Pseudomonas aeruginosa airway infection and lung function decline in children with cystic fibrosis. *Journal of Cystic Fibrosis* **21**, 45–51 (2022).
14. Gellatly, S. L. & Hancock, R. E. W. *Pseudomonas aeruginosa* : new insights into pathogenesis and host defenses. *Pathogens Disease* **67**, 159–173 (2013).
15. La Rosa, R., Johansen, H. K. & Molin, S. Adapting to the Airways: Metabolic Requirements of Pseudomonas aeruginosa during the Infection of Cystic Fibrosis Patients. *Metabolites* **9**, 234 (2019).
16. Pedersen, B. H. *et al.* Metabolic specialization drives reduced pathogenicity in Pseudomonas aeruginosa isolates from cystic fibrosis patients. *PLoS Biol* **22**, e3002781 (2024).
17. Rossi, E. *et al.* Pseudomonas aeruginosa adaptation and evolution in patients with cystic fibrosis. *Nat Rev Microbiol* **19**, 331–342 (2021).
18. Cramer, N. *et al.* Microevolution of the major common *Pseudomonas aeruginosa* clones C and PA14 in cystic fibrosis lungs. *Environmental Microbiology* **13**, 1690–1704 (2011).

19. Fischer, S., Dethlefsen, S., Klockgether, J. & Tümmler, B. Phenotypic and Genomic Comparison of the Two Most Common ExoU-Positive Pseudomonas aeruginosa Clones, PA14 and ST235. *mSystems* **5**, e01007-20 (2020).
20. Jelsbak, L. *et al.* Molecular Epidemiology and Dynamics of *Pseudomonas aeruginosa* Populations in Lungs of Cystic Fibrosis Patients. *Infect Immun* **75**, 2214–2224 (2007).
21. Markussen, T. *et al.* Environmental Heterogeneity Drives Within-Host Diversification and Evolution of Pseudomonas aeruginosa. *mBio* **5**, e01592-14 (2014).
22. Romling, U., Kader, A., Sriramulu, D. D., Simm, R. & Kronvall, G. Worldwide distribution of Pseudomonas aeruginosa clone C strains in the aquatic environment and cystic fibrosis patients. *Environ Microbiol* **7**, 1029–1038 (2005).
23. Weimann, A. *et al.* Evolution and host-specific adaptation of *Pseudomonas aeruginosa*. *Science* **385**, eadi0908 (2024).
24. Yang, L. *et al.* Evolutionary dynamics of bacteria in a human host environment. *Proc. Natl. Acad. Sci. U.S.A.* **108**, 7481–7486 (2011).
25. Bjarnsholt, T. *et al.* The importance of understanding the infectious microenvironment. *The Lancet Infectious Diseases* **22**, e88–e92 (2022).
26. Muggeo, A., Coraux, C. & Guillard, T. Current concepts on Pseudomonas aeruginosa interaction with human airway epithelium. *PLoS Pathog* **19**, e1011221 (2023).
27. Prytherch, Z. *et al.* Tissue-Specific Stem Cell Differentiation in an in vitro Airway Model. *Macromolecular Bioscience* **11**, 1467–1477 (2011).
28. Silva, S., Bicker, J., Falcão, A. & Fortuna, A. Air-liquid interface (ALI) impact on different respiratory cell cultures. *European Journal of Pharmaceutics and Biopharmaceutics* **184**, 62–82 (2023).

29. Goltermann, L. *et al.* Macrolide resistance through uL4 and uL22 ribosomal mutations in Pseudomonas aeruginosa. *Nat Commun* **15**, 8906 (2024).
30. Laborda, P. *et al.* Mutations in the efflux pump regulator MexZ shift tissue colonization by Pseudomonas aeruginosa to a state of antibiotic tolerance. *Nat Commun* **15**, 2584 (2024).
31. Lewin, G. R. *et al.* Application of a quantitative framework to improve the accuracy of a bacterial infection model. *Proc. Natl. Acad. Sci. U.S.A.* **120**, e2221542120 (2023).
32. Swart, A. L. *et al.* Pseudomonas aeruginosa breaches respiratory epithelia through goblet cell invasion in a microtissue model. *Nat Microbiol* **9**, 1725–1737 (2024).
33. Tang, M. *et al.* Evaluating Bacterial Pathogenesis Using a Model of Human Airway Organoids Infected with Pseudomonas aeruginosa Biofilms. *Microbiol Spectr* **10**, e02408-22 (2022).
34. Pleguezuelos-Manzano, C. *et al.* Dual RNA sequencing of a co-culture model of Pseudomonas aeruginosa and human 2D upper airway organoids. *Sci Rep* **15**, 2222 (2025).
35. Walters, M. S. *et al.* Generation of a human airway epithelium derived basal cell line with multipotent differentiation capacity. *Respir Res* **14**, 135 (2013).
36. Espaillat, A. *et al.* Adaptive Evolution of *Pseudomonas aeruginosa* in Human Airways Shows Phenotypic Convergence Despite Diverse Patterns of Genomic Changes. *Molecular Biology and Evolution* **41**, msae022 (2024).
37. Marvig, R. L., Sommer, L. M., Molin, S. & Johansen, H. K. Convergent evolution and adaptation of Pseudomonas aeruginosa within patients with cystic fibrosis. *Nat Genet* **47**, 57–64 (2015).

38. Balasubramanian, D., Schneper, L., Kumari, H. & Mathee, K. A dynamic and intricate regulatory network determines Pseudomonas aeruginosa virulence. *Nucleic Acids Research* **41**, 1–20 (2013).

39. Brencic, A. & Lory, S. Determination of the regulon and identification of novel mRNA targets of *Pseudomonas aeruginosa* RsmA. *Molecular Microbiology* **72**, 612–632 (2009).

40. Moradali, M. F., Ghods, S. & Rehm, B. H. A. Pseudomonas aeruginosa Lifestyle: A Paradigm for Adaptation, Survival, and Persistence. *Front. Cell. Infect. Microbiol.* **7**, (2017).

41. Polack, B., Dacheux, D., Delic-Attree, I., Toussaint, B. & Vignais, P. M. ThePseudomonas aeruginosa fumcandsodaGenes Belong to an Iron-Responsive Operon. *Biochemical and Biophysical Research Communications* **226**, 555–560 (1996).

42. Arai, H. Regulation and Function of Versatile Aerobic and Anaerobic Respiratory Metabolism in Pseudomonas aeruginosa. *Front. Microbio.* **2**, (2011).

43. Shao, X. *et al.* The transcriptional regulators of virulence for Pseudomonas aeruginosa: Therapeutic opportunity and preventive potential of its clinical infections. *Genes & Diseases* **10**, 2049–2063 (2023).

44. Fenn, S. *et al.* NirA Is an Alternative Nitrite Reductase from Pseudomonas aeruginosa with Potential as an Antivirulence Target. *mBio* **12**, e00207-21 (2021).

45. Thuenauer, R. *et al.* The Pseudomonas aeruginosa Lectin LecB Causes Integrin Internalization and Inhibits Epithelial Wound Healing. *mBio* **11**, e03260-19 (2020).

46. Camus, L., Vandenesch, F. & Moreau, K. From genotype to phenotype: adaptations of Pseudomonas aeruginosa to the cystic fibrosis environment. *Microbial Genomics* **7**, (2021).

47. Rossi, E., Falcone, M., Molin, S. & Johansen, H. K. High-resolution in situ transcriptomics of Pseudomonas aeruginosa unveils genotype independent patho-phenotypes in cystic fibrosis lungs. *Nat Commun* **9**, 3459 (2018).

48. Losol, P. *et al.* Bronchial epithelial cells release inflammatory markers linked to airway inflammation and remodeling in response to TLR5 ligand flagellin. *World Allergy Organization Journal* **16**, 100786 (2023).

49. Tseng, J., Do, J., Widdicombe, J. H. & Machen, T. E. Innate immune responses of human tracheal epithelium to Pseudomonas aeruginosa flagellin, TNF-α, and IL-1β. *American Journal of Physiology-Cell Physiology* **290**, C678–C690 (2006).

50. Jurado-Martín, I., Sainz-Mejías, M. & McClean, S. Pseudomonas aeruginosa: An Audacious Pathogen with an Adaptable Arsenal of Virulence Factors. *IJMS* **22**, 3128 (2021).

51. Roberts, N., Al Mubarak, R., Francisco, D., Kraft, M. & Chu, H. W. Comparison of paired human nasal and bronchial airway epithelial cell responses to rhinovirus infection and IL-13 treatment. *Clinical & Translational Med* **7**, e13 (2018).

52. Pesce, E. *et al.* The Autophagy Inhibitor Spautin-1 Antagonizes Rescue of Mutant CFTR Through an Autophagy-Independent and USP13-Mediated Mechanism. *Front. Pharmacol.* **9**, 1464 (2018).

53. Pedemonte, N. *et al.* Discovery of a picomolar potency pharmacological corrector of the mutant CFTR chloride channel. *Sci. Adv.* **6**, eaay9669 (2020).

54. Gianotti, A., Delpiano, L. & Caci, E. In vitro Methods for the Development and Analysis of Human Primary Airway Epithelia. *Front. Pharmacol.* **9**, 1176 (2018).

55. Meisner, J. & Goldberg, J. B. The Escherichia coli *rhaSR-PrhaBAD* Inducible Promoter System Allows Tightly Controlled Gene Expression over a Wide Range in Pseudomonas aeruginosa. *Appl Environ Microbiol* **82**, 6715–6727 (2016).

56. Westermann, A. J., Gorski, S. A. & Vogel, J. Dual RNA-seq of pathogen and host. *Nat Rev Microbiol* **10**, 618–630 (2012).

57. Rossi, E. *et al*. Widespread alterations in systemic immune profile are linked to lung function heterogeneity and airway microbes in cystic fibrosis. *Journal of Cystic Fibrosis* **23**, 885–895 (2024).

58. Love, M. I., Huber, W. & Anders, S. Moderated estimation of fold change and dispersion for RNA-seq data with DESeq2. *Genome Biol* **15**, 550 (2014).